Abdominal Radiology (2024) 49:1113–1121
https://doi.org/10.1007/s00261-023-04159-7

HEPATOBILIARY

Comparison and optimization of *b* value combinations for diffusion-weighted imaging in discriminating hepatic fibrosis

Jiaoyan Wang[1] · Xue Zhou[2] · Mingrong Yao[1] · Wenli Tan[1] · Songhua Zhan[1] · Kun Liu[3] · Zhen Feng[3] · Huamei Yan[4] · Yongming Dai[5] · Jie Yuan[1]

Received: 29 June 2023 / Revised: 13 December 2023 / Accepted: 16 December 2023 / Published online: 29 January 2024

Abstract

Introduction and objectives Diffusion-weighted imaging (DWI) has shown potential in characterizing hepatic fibrosis. However, there are no widely accepted apparent diffusion coefficient (ADC) values for the *b* value combination. This study aims to determine the optimal high and low *b* values of DWI to assess hepatic fibrosis in patients with chronic liver disease.

Materials and methods The prospective study included 81 patients with chronic liver disease and 21 healthy volunteers who underwent DWI, Magnetic resonance elastography (MRE), and liver biopsy. The ADC was calculated by twenty combinations of nine *b* values (0, 50, 100, 150, 200, 800, 1000, 1200, and 1500 s/mm^2).

Results All ADC values of the healthy volunteers were significantly higher than those of the hepatic fibrosis group (all $P<0.01$). With the progression of hepatic fibrosis, ADC values significantly decreased in *b* value combinations (100 and 1000 s/mm^2, 150 and 1200 s/mm^2, 200 and 800 s/mm^2, and 200 and 1000 s/mm^2). ADC values derived from b values of both 200 and 800 s/mm^2 and 200 and 1000 s/mm^2 were found to be more discriminative for differentiating the stages of hepatic fibrosis. An excellent correlation was between the $ADC_{200–1000}$ value and MRE shear stiffness ($r=-0.750$, $P<0.001$).

Conclusion DWI offers an alternative to MRE as a useful imaging marker for detecting and staging hepatic fibrosis. Clinically, ADC values for *b* values ranging from 200–800 s/mm^2 to 200–1000 s/mm^2 are recommended for the assessment of hepatic fibrosis.

Jiaoyan Wang and Xue Zhou have contributed equally to this work.

✉ Jie Yuan
yuanjie3352@shutcm.edu.cn

[1] Department of Radiology, Shuguang Hospital Affiliated to Shanghai University of Traditional Chinese Medicine, No. 528, Zhangheng Road, Pudong District, Shanghai 201203, China

[2] Department of Radiology, Central Hospital of Jiangjin District and Chongqing University Jiangjin Hospital, Chongqing 402260, China

[3] Department of Pathology, Shuguang Hospital Affiliated to Shanghai University of Traditional Chinese Medicine, Shanghai 201203, China

[4] Clinical Research Center, Shuguang Hospital Affiliated to Shanghai University of Traditional Chinese Medicine, Shanghai 201203, China

[5] MR Collaboration, United Imaging Healthcare, Shanghai 200030, China

Graphical abstract

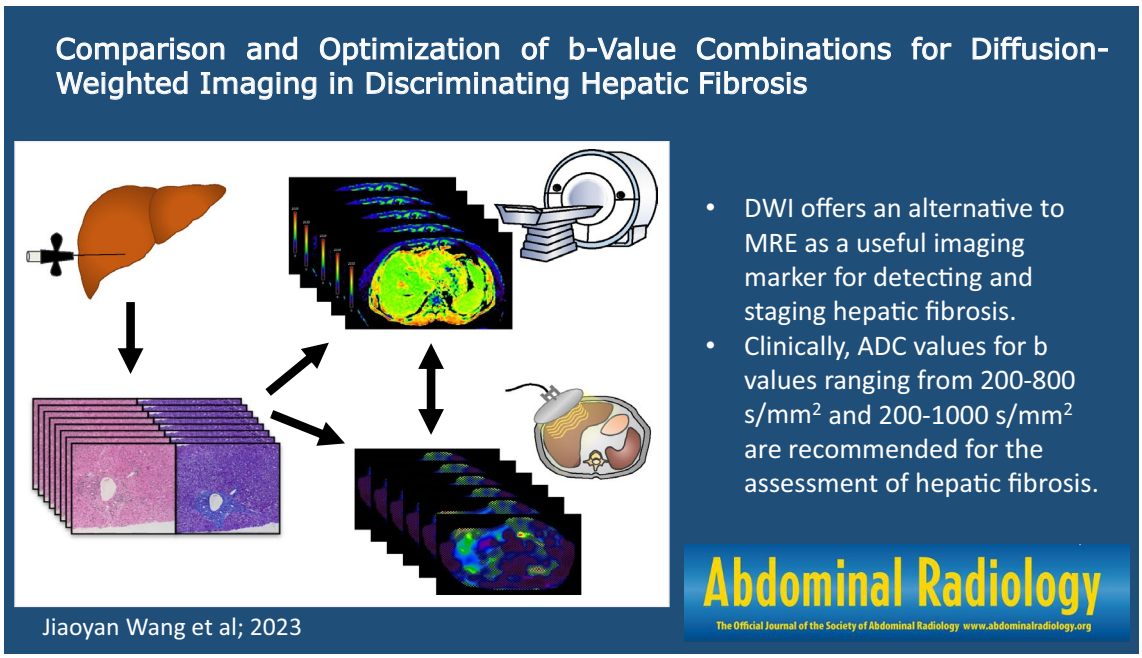

Keywords Diffusion-weighted imaging · Hepatic fibrosis · Magnetic resonance elastography

Introduction

Hepatic fibrosis is a chronic injury caused by various factors such as viral infection, schistosomiasis, alcoholism, and nonalcoholic steatohepatitis, which may eventually lead to irreversible cirrhosis and liver cancer. The primary method for clinically diagnosing hepatic fibrosis is puncture biopsy; however, this invasive procedure may result in serious complications and sampling errors. It is not viewed as an ideal method to accurately reflect the development of hepatic fibrosis [1]. Magnetic resonance elastography (MRE) has been used to measure the mechanical properties of tissues, particularly to detect changes in soft tissues [2]. Owing to its noninvasive nature, MRE can be used as an alternative approach to biopsy for staging hepatic fibrosis [3]. However, the use of external drivers and sophisticated computer processing procedures limit the clinical application of MRE.

Conventional monoexponential diffusion-weighted imaging (DWI) indirectly detects microstructural changes in tissues by measuring both the extent and direction of water molecule diffusion to define the apparent diffusion coefficient (ADC) [4, 5]. In hepatic fibrosis, collagen fibers and cell membranes may block the diffusion of water molecules, resulting in changes in signal intensity and ADC values [6]. Hence, the determination of ADC values using DWI under a diffusion gradient appears to be the most reliable imaging method for evaluating the cumulative effects of water diffusion and capillary perfusion. Previous studies have described the use of DWI as an adjunct to conventional MRI to determine the degree of hepatic fibrosis [7]. Another study demonstrated that ADC calculated by DWI and then converted to a DW MRI-based virtual shear modulus can identify the stage of hepatic fibrosis [8]. Compared with MRE, DWI does not require an external driver for the excitation of shear waveforms, and such diagnostic images are easier to obtain and process. Therefore, DWI presents an alternative to MRE for fibrosis diagnosis, disease progression monitoring, and evaluation of treatment protocols.

ADC values, determined using DWI (and therefore, diagnostic ability), are influenced by *b* value selection. *b* value can reflect the strength and timing of the gradients used to generate DWI. Although DWI is generally viewed as a feasible method to stage hepatic fibrosis in patients, there is no consensus on the optimal combination of high and low *b* values [9]. Hence, this prospective study aimed to detect changes in hepatic fibrosis when DWI is treated as a potential noninvasive biomarker in patients with chronic liver disease and to determine the optimal high and low *b* values for DWI.

Materials and methods

Study population

This single-center, prospective study was approved by the local institutional review board (IRB), and all patients provided signed informed consent to participate in the study.

This study was conducted on 111 subjects divided into two groups. Twenty-one healthy subjects (10 males and 11 females; age range, is from 26 to 65 years; mean age, 44.57 ± 16.06 years) with no history of liver disease, alcohol abuse, liver dysfunction, or liver biopsy were enrolled as controls.

Another 90 cases were patients with known chronic liver disease, identified from local hospital between March 2021 and March 2023. Among them, 81 patients were enrolled in the study after excluding 4 patients due to poor image quality on DWI examination and 5 patients with steatosis or iron overload. There were 50 cases of chronic hepatitis B, 16 of autoimmune hepatitis, 8 of chronic hepatitis C, and 7 of nonalcoholic steatohepatitis, as shown in Table 1. There were 35 males and 46 females with an age range of 24 to 75 years and a mean age of 48.72 ± 12.43 years.

The inclusion criteria were as follows: at least 18 years of age, a history of chronic liver disease, MRI performed prior to liver biopsy, an interval between MRI and biopsy of fewer than 2 months, and the availability of a liver biopsy sample at least 10 mm long.

Table 1 Patient demographics

Parameter	Value
No. of healthy subjects	21
Male	10
Female	11
Mean age (years)	44.57 ± 16.06
No. of patients	81
Male	35
Female	46
Mean age (years)	48.72 ± 12.43
Type of chronic liver disease	
HBV	50
AIH	16
HCV	8
NAFLD	7

HBV hepatitis B virus, *AIH* autoimmune hepatitis, *HCV* hepatitis C virus, *NAFLD* nonalcoholic steatohepatitis

Image acquisition

All MRI examinations were performed with a 3 T scanner (uMR790, United Imaging Medical, Shanghai, China) using a 32-channel body array coil. After at least 8 h off fasting, all patients underwent routine liver MRI sequences, including an axial T1-weighted fast spin-echo sequence (repetition time [TR]/echo time [TE], 3.94 ms/1.41 ms) and an axial T2-weighted fast spin-echo sequence with fat suppression (TR/TE, 9562 ms/97.2 ms).

DWI was acquired based on a single-shot echo-planar imaging sequence (ss-EPI) and the specific scanning parameters were as follows: TR/TE = 3000/67.5 ms, slice thickness = 7 mm, field of view = 380 mm × 280 mm, *b* values were 0, 50, 100, 150, 200, 800, 1000, 1200 and 1500 s/mm^2, and averages were 1, 1, 1, 1, 1, 2, 3, 3, 3. The scan time was 6 min and 21 s.

Two-dimensional (2D) EPI MRE was performed by an active acoustic driver with a 60 Hz frequency to transmit vibrations through a passive pneumatic driver (Resoundant Inc., Rochester, Minnesota). After holding the breath for 10 s at the end of relaxed exhalation, four 10 mm continuous axial images were obtained through the widest transverse section of the liver. The MR scanner automatically processed the wave images into 2D shear stiffness maps.

Image analysis

ADC maps were automatically calculated using MR Image Post-processing Software, Version R005 (United Imaging Medical, Shanghai, China). ADC values were calculated using a monoexponential model for 12 combinations of low and high b values: 0 and 800 s/mm^2, 0 and 1000 s/mm^2, 0 and 1200 s/mm^2, 0 and 1500 s/mm^2, 50 and 800 s/mm^2, 50 and 1000 s/mm^2, 50 and 1200 s/mm^2, 50 and 1500 s/mm^2, 100 and 800 s/mm^2, 100 and 1000 s/mm^2, 100 and 1200 s/mm^2, 100 and 1500 s/mm^2, 150 and 800 s/mm^2, 150 and 1000 s/mm^2, 150 and 1200 s/mm^2, 150 and 1500 s/mm^2, 200 and 800 s/mm^2, 200 and 1000 s/mm^2, 200 and 1200 s/mm^2, 200 and 1500 s/mm^2. The specific formula is as follows:

$$\mathrm{ADC} = \frac{\ln\left(\frac{S1}{S2}\right)}{(b2 - b1)}$$

where $S1$ and $S2$ represent the signal intensities obtained at low and high b values, respectively, and $b1$ and $b2$ are the low and high b values, respectively.

The sex, age, and other information of the patients were all close to the readers. Reader 1 was a senior radiologist with 13 years of experience in abdominal MRI and Reader

Table 2 Mean ± SD for the ADC values calculated by different *b* values combinations

ADC (mm^2/s)	Control	F1	F2	F3	F4
ADC0–800	1725.50 ± 83.74	1535.74 ± 87.01	1486.75 ± 120.72	1414.95 ± 108.96	1431.42 ± 122.51
ADC0–1000	1571.81 ± 84.08	1416.40 ± 99.07	1357.34 ± 98.73	1306.2 ± 69.05	1333.39 ± 110.40
ADC0–1200	1448.74 ± 71.43	1332.66 ± 75.89	1276.09 ± 80.44	1205.75 ± 69.91	1260.19 ± 123.95
ADC0–1500	1306.01 ± 69.81	1210.10 ± 83.23	1164.57 ± 94.41	1125.98 ± 109.81	1163.39 ± 105.84
ADC50–800	1384.54 ± 102.97	1247.83 ± 77.65	1230.34 ± 95.33	1194.06 ± 93.82	1164.33 ± 131.11
ADC50–1000	1273.70 ± 74.02	1178.69 ± 75.00	1154.14 ± 90.67	1104.06 ± 77.49	1097.57 ± 121.49
ADC50–1200	1231.90 ± 87.56	1144.14 ± 90.64	1090.95 ± 87.58	1053.31 ± 63.36	1063.56 ± 111.66
ADC50–1500	1119.40 ± 70.11	1048.85 ± 81.46	1006.46 ± 113.75	990.21 ± 93.32	981.71 ± 94.40
ADC100–800	1349.19 ± 79.34	1239.05 ± 96.85	1208.11 ± 102.08	1181.82 ± 78.99	1142.43 ± 112.76
ADC100–1000	1278.18 ± 58.75	1164.00 ± 94.79	1120.03 ± 85.78	1094.64 ± 87.71	1058.47 ± 91.17
ADC100–1200	1212.82 ± 67.25	1111.26 ± 48.83	1048.95 ± 102.23	1027.15 ± 79.56	1044.67 ± 82.63
ADC100–1500	1120.31 ± 71.67	1032.69 ± 60.72	981.62 ± 98.98	971.66 ± 85.24	944.13 ± 95.22
ADC150–800	1313.78 ± 86.33	1280.69 ± 92.59	1185.46 ± 126.63	1190.90 ± 76.36	1169.47 ± 121.05
ADC150–1000	1248.42 ± 60.71	1171.03 ± 83.05	1114.12 ± 102.83	1107.37 ± 102.54	1074.68 ± 89.58
ADC150–1200	1188.17 ± 65.95	1122.07 ± 68.92	1045.62 ± 96.20	1037.60 ± 99.35	1015.03 ± 87.43
ADC150–1500	1099.35 ± 59.68	1017.11 ± 71.42	961.14 ± 95.65	973.00 ± 81.17	950.17 ± 61.24
ADC200–800	1352.14 ± 67.42	1261.11 ± 82.50	1204.83 ± 90.56	1145.54 ± 104.67	1092.23 ± 133.10
ADC200–1000	1250.79 ± 60.50	1149.23 ± 80.92	1102.92 ± 83.28	1058.93 ± 70.19	1021.65 ± 84.03
ADC200–1200	1173.80 ± 63.65	1104.43 ± 72.94	1022.88 ± 91.94	1008.87 ± 59.76	990.75 ± 72.71
ADC200–1500	1085.45 ± 48.46	1006.80 ± 58.46	937.25 ± 94.59	946.88 ± 84.49	931.65 ± 64.08

2 was a senior radiologist with 12 years of experience in abdominal MRI. Both of them evaluated the images together to determine the regions of interest (ROIs). To keep the size of the ROIs as large as possible, the two readers tried to alleviate possible artifacts when delineating the ROI, which includes the avoidance of the liver edge, large blood vessels (> 3 mm), left lobe (which can be easily affected by heartbeat), and the interference of multi-channel waves. Each ROI was copied to ensure that they had the same size in the same position, which helped to precisely obtain the ADC values at different *b* values. The ROIs of MRE and DWI were delineated in the same level as far as possible.

Liver biopsy

Percutaneous ultrasound-guided liver biopsies were performed by hepatologists in accordance with local standard procedures. All histological specimens were scored by two liver pathologists (Reader 3 with 16 years of experience and Reader 4 with 12 years of experience) who were not aware of any other data. All biopsy samples were stained with hematoxylin–eosin and masson trichrome.

Fibrosis was evaluated semi-quantitatively using the METAVIR scoring system [10]. Fibrosis degree gradings were identified as follows: F0, no fibrosis; F1, portal fibrosis without septa formation; F2, portal fibrosis with few septa; F3, numerous septa without cirrhosis; F4, cirrhosis. All cases in which the two pathologists had different final grades of hepatic fibrosis were reassessed and scored consistently.

Statistical analysis

Data analysis was conducted using IBM SPSS Statistics for Windows, version 21.0 (IBM Corp, Armonk, NY, USA). The measurement data are expressed as the mean ± standard deviation (SD). The Shapiro–Wilk test was used to test the normality of ADC values and MRE stiffness values, and the independent sample *t* test was used to measure the difference in ADC values, which were calculated using different combinations of *b* values separately from the groups of volunteers and patients with chronic liver disease. One-way analysis of variance (ANOVA) was used to compare ADC values at different stages of hepatic fibrosis. The diagnostic performance of ADC values calculated using different *b* value combinations was assessed by considering the area under the receiver operating characteristic curves (AUROCs) during hepatic fibrosis staging. The relationships between ADC values and MRE parameters were investigated using Spearman's correlation. A correlation coefficient classification greater than 0.70 is considered to have an excellent correlation. In this study, $P < 0.01$ was considered statistically significant.

Results

Histological quantification of the fibrosis stage was performed in 81 patients with chronic hepatic disease using biopsy. The results showed that the mean biopsy length was 14.17 ± 2.85 mm, and its range was from 10 to 22 mm. The distribution of fibrosis stages was as follows: F1, $n = 24$; F2, $n = 26$; F3, $n = 16$; and F4, $n = 15$. Table 2 displays the mean ADC values of different combinations of b values from healthy volunteers and patients with different stages of hepatic fibrosis. It is evident that all ADC values from different b value combinations of the healthy volunteers were significantly higher than those of the group with hepatic fibrosis (all $P < 0.01$).

The results also showed that there were significant differences between the ADC values derived from different combinations of b values and hepatic fibrosis stages with all $P < 0.01$ (that is, 0 and 800 s/mm^2, 0 and 1000 s/mm^2, 0 and 1200 s/mm^2, 50 and 1200 s/mm^2, 100 and 1000 s/mm^2, 100 and 1200 s/mm^2, 150 and 800 s/mm^2, 150 and 1200 s/mm^2, 200 and 800 s/mm^2, 200 and 1000 s/mm^2, 200 and 1200 s/mm^2, 200 and 1500 s/mm^2, all $P < 0.01$). With progressing hepatic fibrosis, ADC values significantly decreased in the combinations of b values of 100 and 1000 s/mm^2, 150 and 1200 s/mm^2, 200 and 800 s/mm^2, and 200 and 1000 s/mm^2, as shown in Fig. 1. The combinations of b values of 200 and 800 s/mm^2 and 200 and 1000 s/mm^2 can better distinguish different stages of fibrosis. There were no significant differences between the ADC values and fibrosis stages (that is, 0 and 1500 s/mm^2, 50 and 800 s/mm^2, 50 and 1000 s/mm^2, 50 and 1500 s/mm^2, 100 and 800 s/mm^2, 100 and 1500 s/mm^2, 150 and 1000 s/mm^2, 150 and 1500 s/mm^2, all $P > 0.01$).

Significant predictive values were found for $ADC_{100–1000}$, $ADC_{150–1200}$, $ADC_{200–800,}$ and $ADC_{200–1000}$ which presented diagnostic values with areas under the receiver operating characteristic curves (AUROCs) of 0.693, 0.785, 0.774, and 0.756 for distinguishing METAVIR F1 and F2–4, respectively. The AUROCs for $ADC_{100–1000}$, $ADC_{150–1200}$, $ADC_{200–800}$, and $ADC_{200–1000}$ in the prediction of hepatic fibrosis stages F1–2 and F3–4 were 0.713, 0.680, 0.802, and 0.769, respectively. Significant predictive values were found for $ADC_{100–1000}$, $ADC_{150–1200}$, $ADC_{200–800,}$ and $ADC_{200–1000}$ which presented diagnostic values with AUROCs of 0.728, 0.705, 0.834, and 0.779 for distinguishing F1–3 and F4, respectively. The receiver operating characteristics for the measured data with AUROCs are shown in Fig. 2 and Table 3, respectively.

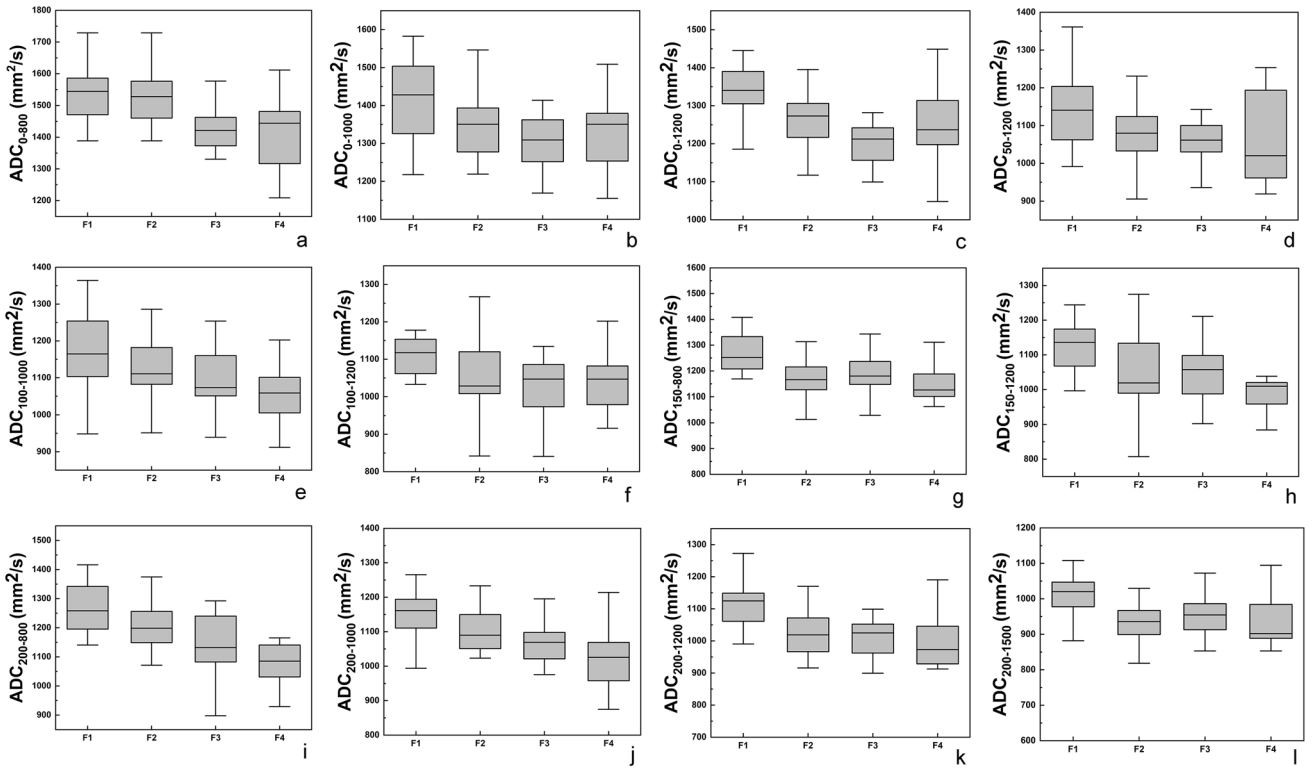

Fig. 1 Box plots of ADC values calculated by difference b values combinations including 0 and 800 s/mm^2 (**A**), 0 and 1000 s/mm^2 (**B**), 0 and 1200 s/mm^2 (**C**), 50 and 1200 s/mm^2 (**D**), 100 and 1000 s/mm^2 (**E**), 100 and 1200 s/mm^2 (**F**), 150 and 800 s/mm^2 (**G**), 150 and 1200 s/mm^2 (**H**), 200 and 800 s/mm^2 (**I**), 200 and 1000 s/mm^2 (**J**), 200 and 1200 s/mm^2 (**K**), 200 and 1500 s/mm^2 (**L**) for the groups F1, F2, F3 and F4

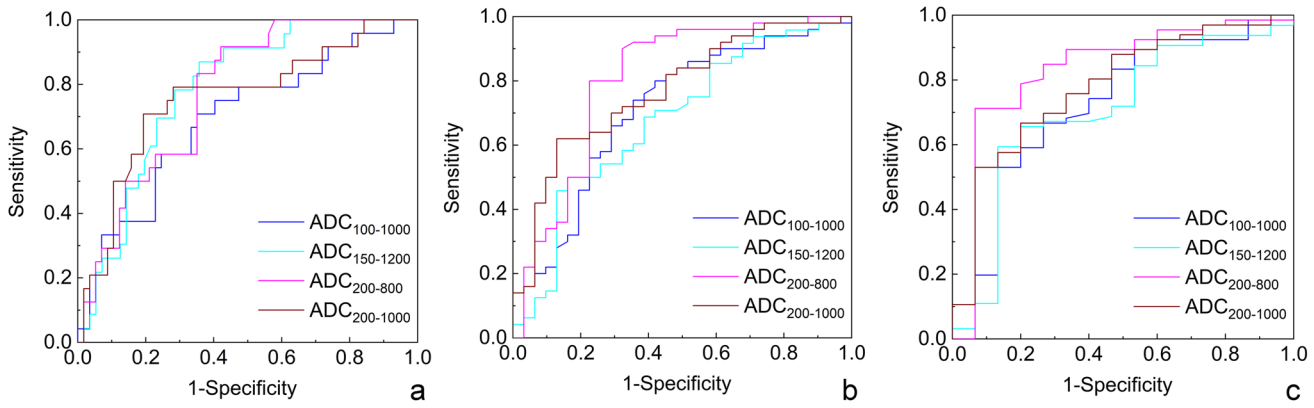

Fig. 2 Receiver operating characteristic curves of $ADC_{100–1000}$, $ADC_{150–1200}$, $ADC_{200–800}$ and $ADC_{200–1000}$ for the detection of hepatic fibrosis stages F1 and F2–4 (**A**), F1–2 and F3–4 (**B**) and fibrosis F1–3 and F4 (**C**)

Table 3 Receiver operating characteristics for measured data with the area under the receiver operating characteristic curves (AUROCs)

Parameters	Cut-off	Sensitivity (%)	Specificity (%)	AUC (95% CI)
F1 versus F2–4				
$ADC_{100–1000}$	1118.80	70.83	64.91	0.693 (0.569–0.818)
$ADC_{150–1200}$	1066.20	78.26	71.43	0.785 (0.659–0.910)
$ADC_{200–800}$	1171.05	91.67	57.90	0.774 (0.651–0.896)
$ADC_{200–1000}$	1125.15	70.83	80.70	0.756 (0.640–0.872)
F1–2 versus F3–4				
$ADC_{100–1000}$	1085.10	64.52	74.00	0.713 (0.597–0.828)
$ADC_{150–1200}$	1101.85	50.00	83.87	0.680 (0.559–0.800)
$ADC_{200–800}$	1142.45	90.0	67.74	0.802 (0.705–0.899)
$ADC_{200–1000}$	1104.20	62.0	87.10	0.769 (0.662–0.876)
F1–3 versus F4				
$ADC_{100–1000}$	1118.80	53.03	86.67	0.728 (0.588–0.868)
$ADC_{150–1200}$	1022.85	65.63	80.00	0.705 (0.555–0.854)
$ADC_{200–800}$	1166.50	71.21	93.33	0.834 (0.716–0.951)
$ADC_{200–1000}$	1070.75	66.67	80.00	0.779 (0.647–0.911)

The correlations were statistically significant between MRE shear stiffness and ADC values obtained using DWI for all *b*-value combinations in all subjects (all $P<0.001$). There were excellent correlations between MRE shear stiffness and ADC values ($b=0$ and 800 s/mm^2, $b=200$ and 1000 s/mm^2, $b=200$ and 1200 s/mm^2) ($r=-0.707$, -0.750, -0.709, respectively; all $P<0.001$), as shown in Figs. 3 and 4. ADC values derived using *b* 200 and 1000 s/mm^2 exhibited the most significant correlation with MRE.

Discussion

Liver fibrosis caused by chronic liver disease is mainly manifested by excessive deposition of collagen in the extracellular matrix. DWI is very sensitive to tissue components such as cells, fibers, and interstitium [11]. Therefore, it has potential applications in the field of fibrosis assessment in patients with chronic liver disease [12]. The choice of *b* value is very important in DWI. In this study, we used nine *b* values for DWI and obtained twenty ADC values for the evaluation of hepatic fibrosis. Then, the ADC values and degree of hepatic fibrosis through liver tissue puncture were analyzed.

It was found that the two combinations of *b* values of 200 and 800 s/mm^2 and 200 and 1000 s/mm^2 could better identify the stages of hepatic fibrosis. This significant correlation was not unexpected, because the same microstructural changes were generally based on DWI measurements. Factors including tissue fibers, water molecule movement, and alterations in cell function can interact to cause these changes. If hepatic fibrosis occurs, extracellular collagen fiber deposition increases with cell damage, atrophy,

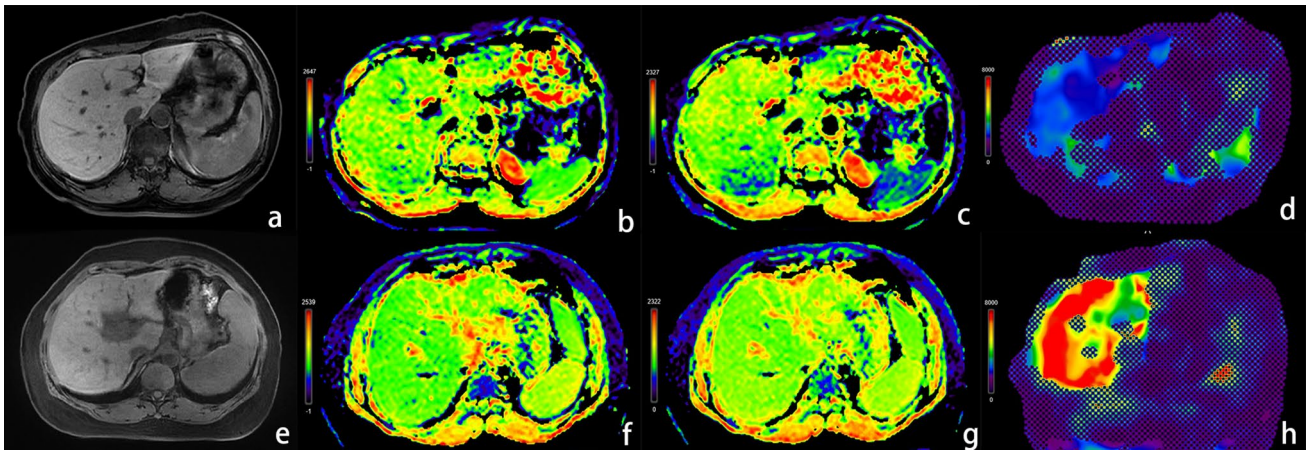

Fig. 3 A 63-year-old female health volunteer (**A**–**D**) and a 51-year-old female with chronic hepatitis B with F4 hepatic fibrosis (**E**–**H**). **A** and **E** showed T1-weighted maps. **B** and **F** showed ADC maps using the *b* values between 200 and 800 s/mm^2. **C** and **G** showed ADC maps using the *b* values between 200 and 1000 s/mm^2. **D** and **H** showed the elastogram

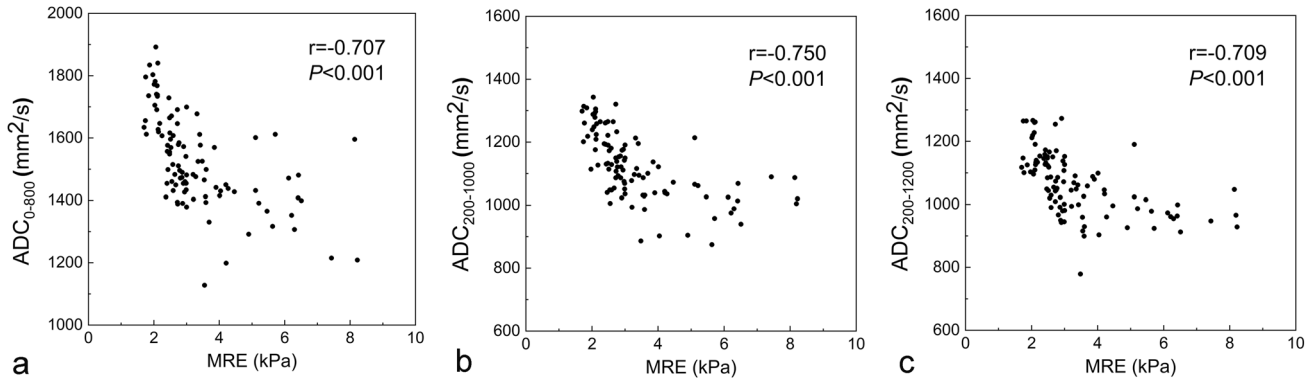

Fig. 4 Graphs of the results of correlation between ADC values and MRE shear modulus. Using the *b* values between 0 and 800 s/mm^2, 200 and 1000 s/mm^2, 200 and 1200 s/mm^2, ADC all had significant correlation with MRE shear modulus (all $P < 0.01$)

and necrosis, resulting in an increase in liver cirrhosis. Fibrotic changes also narrow the gaps between tissue cells and reduce cell permeability, thereby limiting the diffusion of water molecules in and out of the cells and changing the concentrations of enzymes. Thus, there is a common physiological, pathological, and histological basis for the movement of water molecules and tissue hardness [13, 14].

Diffusion-weighted magnetic resonance imaging (DWI) is very sensitive to the diffusion motion of water molecules and can be used to quantify changes in the motion of water molecules in physiological and pathological states [15]. Therefore, it is not surprising that they are closely associated with hepatic fibrosis. Our study found that ADC values decreased with an increase in fibrosis scores, which is consistent with a previous study by Lewin et al. [7]. Furthermore, the mean ADC values in all different *b* value combinations were significantly higher in the group of healthy volunteers than that in F1–4 patients. These results further support the view that DWI can be used to evaluate the stage of hepatic fibrosis.

The choice of the *b* value is very important in DWI. Previous studies have shown that small *b* values (less than 200 s/mm^2) mainly reflect changes in tissue perfusion. The smaller the *b* value, the greater the perfusion effect. However, larger *b* values (> 200 s/mm^2) mainly reflect the dispersion state of water molecules, and the larger the value of *b*, the greater the proportion of dispersion [16]. In this study, we mainly adopted a spin-plane echo sequence with 20 sets of *b* values for DWI. It has been shown that the optimal clinical image of the liver can be obtained when the *b* value combinations are 200–800 s/mm^2 and 200–100 s/mm^2, respectively.

The diagnostic performance of DWI at different stages of hepatic fibrosis is acceptable. Previous studies have suggested that the diagnostic performance of DWI is similar to that of transient elastic imaging, FibroScan, platelet ratio index (APRI), fibrosis index based on the four

factors (FIB-4), and serum hyaluronate [7, 17]. In F0–2 vs F3–4, the AUROCs of Fibroscan was 0.85 in patients with hepatitis C infection [18]. A meta-analysis showed the AUROCs of APRI and FIB-4 for the diagnosis of significant fibrosis were 0.7407 and 0.7844 [19]. Although DWI is less effective than MRE for diagnosis [20], compared with MRE, DWI only needs to calculate two *b* values, which greatly reduces the time cost. Moreover, there is no need for external drivers, which reduces instrumentation costs. The post-processing method is also simpler, reducing the probability of errors. Therefore, virtual elastography based on diffusion-weighted imaging has clinical significance for the quantitative evaluation of hepatic fibrosis. Our study found that all ADC values derived from twenty *b* value combinations were correlated with MRE. Among them, the $ADC_{0–800}$, $ADC_{200–1000,}$ and $ADC_{200–1200}$ values have a better correlation with MRE. Compared with MRE, DWI only needs to calculate two *b* values, which greatly reduces the time cost. Moreover, there is no need for external drivers, which reduces instrumentation cost. The post-processing method is also simpler, reducing the probability of errors. Therefore, DWI can be used as an alternative to MRE to evaluate the degree of hepatic fibrosis.

In this study, the AUROC values of ADC values calculated by the *b*-value combinations of 200–800 s/mm^2 and 200–1000 s/mm^2 were all greater than 0.750 for the recognition of hepatic fibrosis in the F1 and F2–4 groups, F1–2 and F3–4 groups, and F1–3 and F4 groups, respectively. The ADC values calculated using *b* values of 200 and 800 s/mm^2 had better sensitivity and specificity for fibrosis stages than the *b* values of 200 and 1000 s/mm^2. It has been shown that the optimal clinical image of the liver can be obtained when the *b* value is 800 s/mm^2 and in this way, it can meet clinical requirements. Furthermore, the post-processing method is simple, which helps reduce the probability of errors. Therefore, DWI is clinically important for the evaluation of hepatic fibrosis.

This study collected the ADC values derived from different b-value combinations from 81 patients with chronic liver disease and 21 healthy volunteers. The number of samples was large and the experimental results were reliable. This method is useful for the characterization of hepatic fibrosis. Since various pathological changes affect the state of tissue diffusion, this feature can be utilized to further assess the physical condition of an organ that is affected by diseases, and thus provide more practical methods for clinical diagnosis of these diseases. This study still has some limitations. First of all, this study is limited to our single-center study, and we need more center studies in the future to further verify the results of this study in the future. Secondly, when selecting MRE and ADC ROIs, we tried our best to select similar positions, but the point-to-point accurate matching was still not achieved. It is necessary to accurately locate puncture and MRI images in future studies. Third, DWI still has its limitations, especially the signal-to-noise ratio decreases and motion artifacts increase at high *b*-values, so we need to further optimize the scanning parameters in the future.

Conclusions

In conclusion, we found that the technique based on DWI can characterize hepatic fibrosis and provide more information on the degree of hepatic fibrosis in this study. Clinically, two combinations of *b* values of 200–800 s/mm^2 and 200–1000 s/mm^2 are recommended for the assessment of hepatic fibrosis. Among them, it is best for *b* values of 200 and 800 s/mm^2.

Funding None.

Data availability Data can be made available upon reasonable request to the senior author.

Declarations

Conflict of interest None.

References

1. Gilmore IT, Burroughs A, Murray-Lyon IM, Williams R, Jenkins D, Hopkins A (1995) Indications, methods, and outcomes of percutaneous liver biopsy in England and Wales: an audit by the British Society of Gastroenterology and the Royal College of Physicians of London. Gut 36(3):437–441. https://doi.org/10.1136/gut.36.3.437
2. Idilman IS, Li J, Yin M, Venkatesh SK (2020) MR elastography of liver: current status and future perspectives. Abdominal radiology (New York) 45(11):3444–3462. https://doi.org/10.1007/s00261-020-02656-7
3. Morisaka H, Motosugi U, Ichikawa S, Nakazawa T, Kondo T, Funayama S, Matsuda M, Ichikawa T, Onishi, H (2018) Magnetic resonance elastography is as accurate as liver biopsy for liver fibrosis staging. Journal of magnetic resonance imaging: JMRI 47(5):1268–1275. https://doi.org/10.1002/jmri.25868
4. Taouli B, Koh DM (2010) Diffusion-weighted MR imaging of the liver. Radiology 254(1):47–66. https://doi.org/10.1148/radiol.09090021
5. Shenoy-Bhangle A, Baliyan V, Kordbacheh H, Guimaraes AR, Kambadakone, A (2017) Diffusion weighted magnetic resonance imaging of liver: Principles, clinical applications and recent updates. World journal of hepatology 9(26):1081–1091. https://doi.org/10.4254/wjh.v9.i26.1081
6. Mathew RP, Venkatesh SK (2018) Imaging of Hepatic Fibrosis. Current gastroenterology reports 20(10):45. https://doi.org/10.1007/s11894-018-0652-7
7. Lewin M, Poujol-Robert A, Boëlle PY, Wendum D, Lasnier E, Viallon M, Guéchot J, Hoeffel C, Arrivé L, Tubiana JM, Poupon R (2007) Diffusion-weighted magnetic resonance imaging for the assessment of fibrosis in chronic hepatitis C. Hepatology

(Baltimore, Md.) 46(3):658–665. https://doi.org/10.1002/hep.21747
8. Kromrey ML, Le Bihan D, Ichikawa S, Motosugi U (2020) Diffusion-weighted MRI-based Virtual Elastography for the Assessment of Liver Fibrosis. Radiology 295(1):127–135. https://doi.org/10.1148/radiol.2020191498
9. Petitclerc L, Sebastiani G, Gilbert G, Cloutier G, Tang A (2017) Liver fibrosis: Review of current imaging and MRI quantification techniques. Journal of magnetic resonance imaging: JMRI 45(5):1276–1295. https://doi.org/10.1002/jmri.25550
10. Intraobserver and interobserver variations in liver biopsy interpretation in patients with chronic hepatitis C (1994) The French METAVIR Cooperative Study Group. Hepatology (Baltimore, Md.) 20(1):15–20.
11. Alkalay RN, Burstein D, Westin CF, Meier D, Hackney DB (2015) MR diffusion is sensitive to mechanical loading in human intervertebral disks ex vivo. Journal of magnetic resonance imaging : JMRI 41(3):654-64. https://doi.org/10.1002/jmri.24624
12. Yang L, Rao S, Wang W, Chen C, Ding Y, Yang C, Grimm R, Yan X, Fu C, Zeng M (2018) Staging liver fibrosis with DWI: is there an added value for diffusion kurtosis imaging?. European radiology 28(7):3041–3049. https://doi.org/10.1007/s00330-017-5245-6
13. Sheng RF, Wang HQ, Yang L, Jin KP, Xie YH, Chen CZ, Zeng MS (2017) Diffusion kurtosis imaging and diffusion-weighted imaging in assessment of liver fibrosis stage and necroinflammatory activity. Abdominal radiology (New York) 42(4):1176–1182. https://doi.org/10.1007/s00261-016-0984-4
14. Xie S, Li Q, Cheng Y, Zhou L, Xia S, Li J, Shen W (2020) Differentiating mild and substantial hepatic fibrosis from healthy controls: a comparison of diffusion kurtosis imaging and conventional diffusion-weighted imaging. Acta radiologica (Stockholm, Sweden: 1987) 61(8):1012–1020. https://doi.org/10.1177/0284185119889566
15. Kim CK, Park BK, Kim B (2010) Diffusion-weighted MRI at 3 T for the evaluation of prostate cancer. AJR. American journal of roentgenology 194(6):1461–1469. https://doi.org/10.2214/AJR.09.3654
16. Kaya B, Koc Z (2014) Diffusion-weighted MRI and optimal b-value for characterization of liver lesions. Acta radiologica (Stockholm, Sweden: 1987) 55(5):532–542. https://doi.org/10.1177/0284185113502017
17. Castéra L, Vergniol J, Foucher J, Le Bail B, Chanteloup E, Haaser M, Darriet M, Couzigou P, De Lédinghen V (2005) Prospective comparison of transient elastography, Fibrotest, APRI, and liver biopsy for the assessment of fibrosis in chronic hepatitis C. Gastroenterology 128(2):343–350. https://doi.org/10.1053/j.gastro.2004.11.018
18. Ueda N, Kawaoka T, Imamura M, Aikata H, Nakahara T, Murakami E, Tsuge M, Hiramatsu A, Hayes CN, Yokozaki M, Chayama K (2020) Liver fibrosis assessments using FibroScan, virtual-touch tissue quantification, the FIB-4 index, and mac-2 binding protein glycosylation isomer levels compared with pathological findings of liver resection specimens in patients with hepatitis C infection. BMC gastroenterology 20(1): 314. https://doi.org/10.1186/s12876-020-01459-w
19. Xiao G, Yang J, Yan L (2015) Comparison of diagnostic accuracy of aspartate aminotransferase to platelet ratio index and fibrosis-4 index for detecting liver fibrosis in adult patients with chronic hepatitis B virus infection: a systemic review and meta-analysis. Hepatology (Baltimore, Md.) 61(1): 292–302. https://doi.org/10.1002/hep.27382
20. Wang QB, Zhu H, Liu HL, Zhang B (2012) Performance of magnetic resonance elastography and diffusion-weighted imaging for the staging of hepatic fibrosis: A meta-analysis. Hepatology (Baltimore, Md.) 56(1): 239–247. https://doi.org/10.1002/hep.25610